

# The evolving quality of frictional contact with graphene

Suzhi Li<sup>1,2,3</sup>, Qunyang Li<sup>4,5</sup>, Robert W. Carpick<sup>6</sup>, Peter Gumbsch<sup>7,8</sup>, Xin Z. Liu<sup>6</sup>, Xiangdong Ding<sup>1</sup>, Jun Sun<sup>1,9</sup> & Ju Li<sup>1,2,9</sup>

Graphite and other lamellar materials are used as dry lubricants for macroscale metallic sliding components and high-pressure contacts. It has been shown experimentally that monolayer graphene exhibits higher friction than multilayer graphene and graphite, and that this friction increases with continued sliding, but the mechanism behind this remains subject to debate. It has long been conjectured that the true contact area between two rough bodies controls interfacial friction<sup>1</sup>. The true contact area, defined for example by the number of atoms within the range of interatomic forces, is difficult to visualize directly but characterizes the quantity of contact. However, there is emerging evidence that, for a given pair of materials, the quality of the contact can change, and that this can also strongly affect interfacial friction<sup>2–7</sup>. Recently, it has been found that the frictional behaviour of two-dimensional materials exhibits traits<sup>8–13</sup> unlike those of conventional bulk materials. This includes the abovementioned finding that for few-layer two-dimensional materials the static friction force gradually strengthens for a few initial atomic periods before reaching a constant value. Such transient behaviour, and the associated enhancement of steady-state friction, diminishes as the number of two-dimensional layers increases, and was observed only when the two-dimensional material was loosely adhering to a substrate<sup>8</sup>. This layer-dependent transient phenomenon has not been captured by any simulations<sup>14,15</sup>. Here, using atomistic simulations, we reproduce the experimental observations of layer-dependent friction and transient frictional strengthening on graphene. Atomic force analysis reveals that the evolution of static friction is a manifestation of the natural tendency for thinner and less-constrained graphene to re-adjust its configuration as a direct consequence of its greater flexibility. That is, the tip atoms become more strongly pinned, and show greater synchrony in their stick-slip behaviour. While the quantity of atomic-scale contacts (true contact area) evolves, the quality (in this case, the local pinning state of individual atoms and the overall commensurability) also evolves in frictional sliding on graphene. Moreover, the effects can be tuned by pre-wrinkling. The evolving contact quality is critical for explaining the time-dependent friction of configurationally flexible interfaces.

We conducted molecular dynamics simulations by sliding a silicon tip over graphene supported on an amorphous Si (a-Si) substrate (see Methods). Substrate–graphene adhesion was modelled as a van der Waals interaction with an effective work of adhesion of approximately  $0.1 \text{ J m}^{-2}$ , based on experimental values<sup>16</sup>. Figure 1a shows the relaxed system consisting of a-Si and a monolayer of graphene at 300 K. As in experiments<sup>16</sup>, the modelled surface morphology of graphene conformed well to the a-Si substrate (Fig. 1b and c). A rigid round

(001)-oriented crystalline silicon tip with a radius of 16.3 nm was placed in contact with graphene (Fig. 1d) and equilibrated for 2 ns (Fig. 1e and f). Graphene's high out-of-plane flexibility coupled with tip–graphene adhesion causes local puckering near the contact edge (Fig. 1e, arrow). A similar puckering phenomenon was also found for the multilayer graphene systems (see Supplementary Discussion 1).

We then applied an external normal load of 0.8 nN to the tip and further relaxed the whole system. After relaxation, we displaced a harmonic spring laterally coupled to the tip at  $2 \text{ m s}^{-1}$ . It is noted that the normal load was stably maintained at 0.8 nN during the friction simulation (see Supplementary Discussion 2). As the tip slid on graphene (with layer numbers  $N=1-4$ ), clear stick–slip motion with two distinct stages was observed in all cases (Fig. 1g), in contrast to conventional atomic stick–slip on bulk graphite<sup>17</sup>. Initially, the local peaks of the lateral force (that is, the static friction force, when slip initiates) increased progressively with each slip. After a few periods, the behaviour became regular, and the peak forces remained constant. The slip distance in each stick–slip event is approximately  $2.5 \text{ \AA}$ , equivalent to the lattice spacing of graphene. The simulations consistently reproduce, for the first time, the two-stage friction behaviour observed in experiments<sup>8</sup>.

Our simulations also show layer-dependent friction<sup>8</sup>, that is, the strengthening effect became weaker and the frictional force reduced as sample thickness increased; the strengthening almost vanished once the thickness reached four layers. To check that two-stage friction was not a dynamic effect caused by the high sliding speed, we first reduced the speed to  $1 \text{ m s}^{-1}$  and  $0.5 \text{ m s}^{-1}$  and found that there is only a weak dependence of the frictional strengthening on sliding speed (see Supplementary Discussion 3). In addition, we performed quasi-static calculations<sup>5,18</sup> and found that the two-stage friction trait was retained (see Supplementary Discussion 4). Finally, we computed the energy barriers for stick–slip motion, and confirmed that the stick–slip event is not driven primarily by thermal fluctuations at experimental time and force scales, but primarily by the external forcing (see Supplementary Discussion 5).

Early studies attributed the friction enhancement for thinner two-dimensional samples to puckering<sup>8,14,19</sup>, where the sliding tip induces more out-of-plane deformation for thinner samples, leading to a larger true contact area and thereby a larger friction. Here, we also observed noticeable puckering (Fig. 1e, Supplementary Video) and found that the puckered configuration evolved as the tip moved forward. Figure 1h shows the average friction force together with the contact area in the constant static friction force regime (that is, beyond the initial strengthening regime) for different layered graphene samples. The simulations show that a larger contact area corresponded to larger friction, and was correlated with increased puckering. However, the friction increase

<sup>1</sup>State Key Laboratory for Mechanical Behavior of Materials and Frontier Institute of Science and Technology, Xi'an Jiaotong University, Xi'an 710049, China. <sup>2</sup>Department of Nuclear Science and Engineering and Department of Materials Science and Engineering, Massachusetts Institute of Technology, Cambridge, Massachusetts 02139, USA. <sup>3</sup>Institute of Nanotechnology, Karlsruhe Institute of Technology, 76344 Eggenstein-Leopoldshafen, Germany. <sup>4</sup>Center for Nano and Micro Mechanics, Applied Mechanics Laboratory, School of Aerospace Engineering, Tsinghua University, Beijing 100084, China. <sup>5</sup>State Key Laboratory of Tribology, Tsinghua University, Beijing 100084, China. <sup>6</sup>Department of Mechanical Engineering and Applied Mechanics, University of Pennsylvania, Philadelphia, Pennsylvania 19104, USA. <sup>7</sup>Institute for Applied Materials, Karlsruhe Institute of Technology, 76131 Karlsruhe, Germany. <sup>8</sup>Fraunhofer Institute for Mechanics of Materials IWM, 79108 Freiburg, Germany. <sup>9</sup>Center for Advancing Materials Performance from the Nanoscale (CAMP-Nano), School of Materials Science and Engineering, Xi'an Jiaotong University, Xi'an 710049, China.

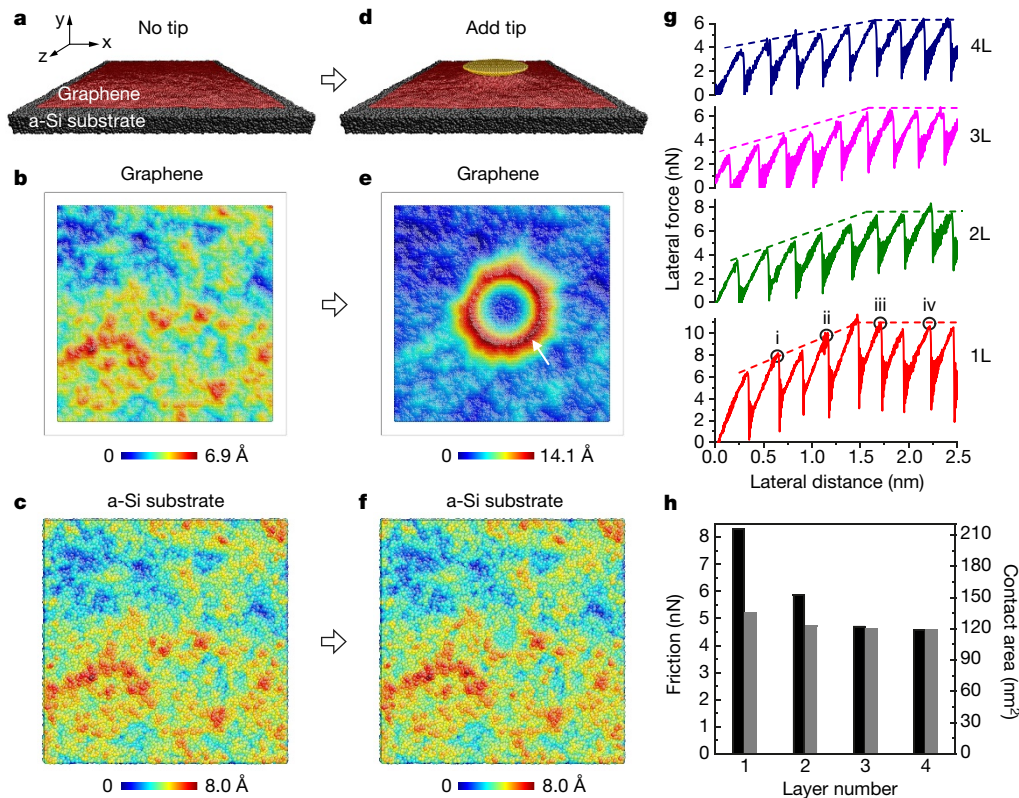


**Figure 1 | Model setup and frictional behaviour for a Si tip sliding over a graphene/a-Si substrate system at 300 K.** **a**, Graphene adhering to the a-Si substrate. **b**, **c**, Surface morphology of monolayer graphene (**b**) and the substrate (**c**). **d**, A rigid Si tip is placed in contact with graphene for the friction tests. **e**, **f**, Morphology of monolayer graphene (**e**) and substrate (**f**) in the presence of the tip after 2 ns. The lateral dimensions of the substrate and graphene are 43.4 nm × 43.4 nm and 38.5 nm × 38.6 nm, respectively. **g**, Force traces showing stick-slip behaviour on single (1L) and multilayer

(an 80% increase for monolayer versus four-layer graphene, consistent with experiments) was substantially larger than the change in contact area (14%). Therefore, the true contact area (which by definition is geometric and additive) change caused by the puckering of graphene alone cannot account for the large increase in friction. This strongly suggests the existence of additional mechanisms contributing to the layer dependence of friction and the transient strengthening.

To trace the physical processes at play, we analysed the distribution of atomistic interaction forces at the interface. For the tip, the net lateral interaction force from graphene,  $F_{\text{interact}}$ , is the sum of the  $x$  components of all atomic forces exerted by graphene,  $F_{\text{interact}} = \sum_i f_i^{\text{friction}} = \sum_i (f_i(x_{\text{spr}}) - f_i(0))$ , where  $f_i(x_{\text{spr}})$  is the  $x$  component of the graphene–tip interaction force for tip atom  $i$  when the spring moves a distance  $x_{\text{spr}}$ , and  $f_i(0)$  is the interaction force before sliding. To highlight the resultant forces due to sliding, we considered only the incremental interfacial forces with respect to the initial state (see Supplementary Discussion 6).

We first performed interfacial force analysis for monolayer graphene. Figure 2a–d shows the  $f_i^{\text{friction}}$  distributions at four moments, each when the lateral force reached its local peak values during the stick-slip friction, marked i, ii, iii and iv in Fig. 1g. Owing to the crystallographic and geometrical differences between graphene and silicon,  $f_i^{\text{friction}}$  values at all four moments exhibited a seemingly random distribution; the total sum in each case was negative (thus producing frictional resistance). The  $f_i^{\text{friction}}$  distribution clearly evolved from points i to iii (Fig. 2a–c) and was almost unchanged between points iii and iv (Fig. 2c and d).

We individually followed  $f_i^{\text{friction}}$  of a few tip atoms that were acting as pinning sites or ‘traps’ (see Supplementary Discussion 7). For some of these atoms, the absolute value of  $f_i^{\text{friction}}$  increased in the strengthening

(2L–4L) graphene/a-Si substrates. **h**, Variations of averaged friction (black) and contact area (grey) with number of layers of graphene. The black, red and gold atoms in **a** and **d** refer to the a-Si substrate, graphene and the tip, respectively; atoms in **b**, **c**, **e** and **f** are coloured according to the height amplitude along the  $y$  direction. The tip–graphene contact area is taken to be  $ms$ , where  $m$  is the number of graphene atoms that are in intimate contact with the tip atoms and  $s$  ( $2.77 \text{ \AA}^2$  per atom) is the atomic area of graphene (see Methods for details).

stage and then saturated. This indicates that pinning gets progressively stronger at these sites with each slip. These atoms apparently provide a substantial contribution to frictional strengthening. For most atoms, the variation of  $f_i^{\text{friction}}$  was steady, indicating no pinning enhancement. These atoms contribute to the overall friction, but not to the initial transient strengthening by local trap deepening.

Further inspection shows that the variation of the interfacial force is closely related to the local configuration of the contacting graphene. If the environment near a tip atom allows the graphene to locally adjust its atomic configuration, the interfacial force will exhibit an evolution effect. However, the detailed local contact environment varies from atom to atom owing to complex tip, graphene and rough substrate configurations. We cannot tell beforehand how an individual tip atom and its surrounding would evolve, because they not only depend on the initial configuration but also depend on the randomly rough surface and the complicated deformation history (for example, the statistical features of the final configuration depend on the entire sliding path, and not just on the initial and final tip locations). Nevertheless, our simulations clearly demonstrate that the interface tends to evolve towards a more commensurate (that is, with more atomic alignment at the interface) and better-pinned state (that is, it finds a deeper energy trap).

To quantify this, we plotted the histogram of the atomic interaction forces at these four moments in Fig. 2e. All four histograms have larger populations at low-magnitude interaction forces and much lower populations at high magnitude. However, these histograms were all skewed negatively because the overall net force was negative. More importantly, as indicated by the insets of Fig. 2e, the range of the distribution increased appreciably from points i to iv (for example, the maximum forces are around  $\pm 0.6 \text{ nN}$  at point i, but increase to  $\pm 0.8 \text{ nN}$

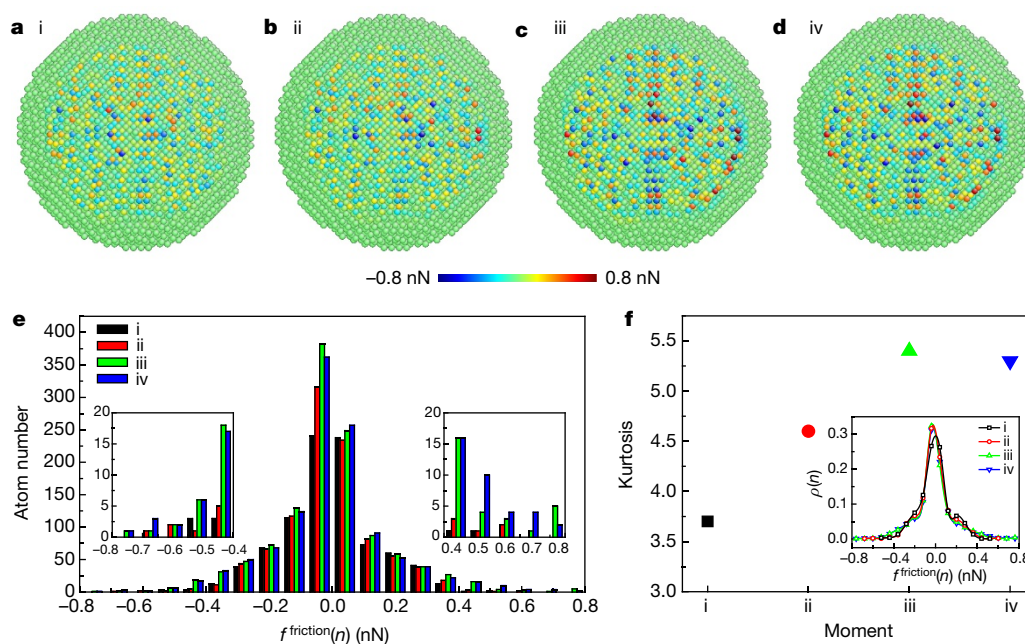


**Figure 2 | Evolution of the atomic-level forces contributing to friction on a monolayer graphene/a-Si substrate. a–d,** Corresponding  $f_i^{\text{friction}}$  distribution at the four moments marked in Fig. 1g. The sites with positive magnitude of  $f_i^{\text{friction}}$  (red colour) are the local pushing points that help the tip slip forward (to the right), while the sites with negative magnitude of  $f_i^{\text{friction}}$  (blue colour) are the local pinning points that produce lateral resistance. **e,** The histogram of  $f_i^{\text{friction}}(n)$  at each of the four moments.

The histogram is obtained by dividing the range of interfacial forces into twenty bins and plotting the number of tip atoms with interaction forces within each bin. The insets provide a magnified view of the distribution in the tails. **f,** The kurtosis value for the four force distributions at the four moments. The inset shows the force distributions that were used to calculate kurtosis.  $\rho(n)$  is the normalized atom number in each corresponding bin of interfacial forces.

at points iii and iv). This local force enhancement is consistent with the higher contrast of interfacial forces shown in Fig. 2a–d, which confirms the abovementioned local trap deepening. In addition, geometrical analysis also suggests that the tip–graphene interface evolved through small atomic shifts to produce more intimate atomic contact as the tip was displaced forward, providing more atomic pinning sites for lateral sliding (see Supplementary Discussion 8).

We further analysed the evolving commensurability of the interface. A less structured contact interface should have a unimodal force

distribution, similar to a Gaussian or even a uniform distribution. A very effective parameter with which to describe the deviation from a unimodal distribution (see Supplementary Discussion 9) is the kurtosis  $K = \mu_4/\sigma^4$ , where  $\mu_4$  is the fourth moment about the mean value and  $\sigma$  is the standard deviation of the distribution (see Methods). The larger  $K$ , the more structured the distribution becomes, and the more commensurate the interface. Figure 2f show the kurtosis values for points i to iv. The kurtosis increased from point i to point iii and was almost unchanged between points iii and iv. This provides an

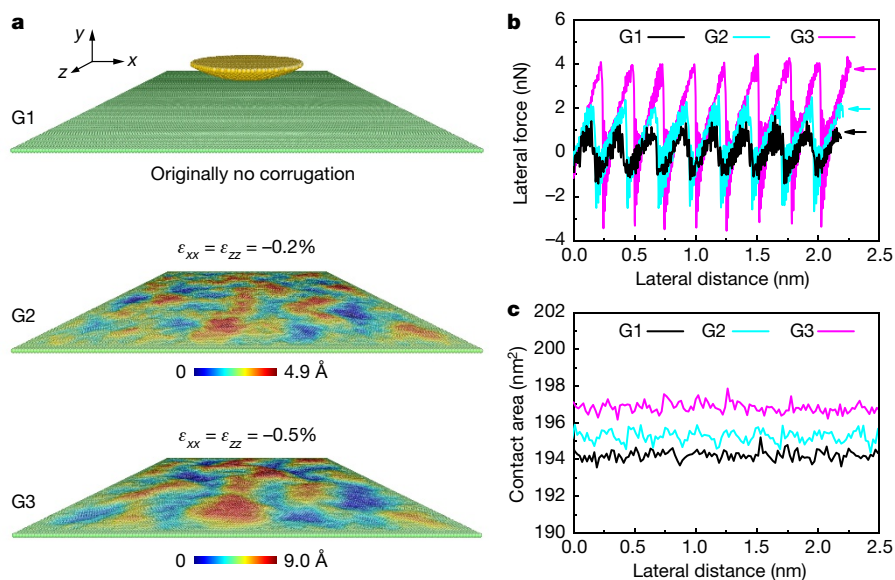


**Figure 3 | Simulations of stick-slip friction on monolayer suspended graphene at 300 K. a,** Simulation model. Three graphene samples with different amounts of pre-existing wrinkles are generated, named G1, G2 and G3. The colours represent the out-of-plane height amplitude.

The induced peak-to-peak height undulations of G2 and G3 are 4.9 Å and 9.0 Å, respectively. **b,** Lateral force traces showing friction sliding on the three samples. **c,** Variation of tip–graphene contact area during sliding.



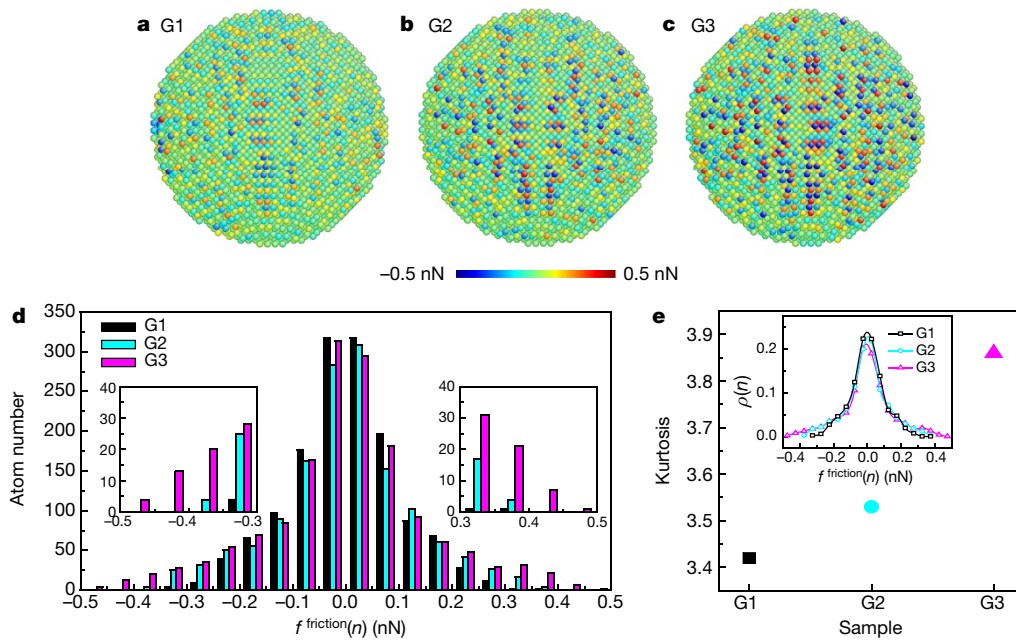


**Figure 4 | Evolution of the atomic-level forces contributing to friction on monolayer suspended graphene.** **a–c**, Comparison of  $f_i^{\text{friction}}$  distribution in the three samples of Fig. 3b. **d**, The histograms of  $f_i^{\text{friction}}(n)$  for the three samples. The insets provide a magnified view of the

distribution in the tails. **e**, The kurtosis value of the distributions of  $f_i^{\text{friction}}(n)$  for the three samples. The inset shows the force distributions that were used to calculate the kurtosis.  $\rho(n)$  is the normalized atom number in each corresponding bin of interfacial forces.

indication that the tip–graphene interface became slightly more commensurate with each slip initially, and finally reached a stable value.

The simulations unambiguously show that the friction strengthening originates from two key mechanisms: enhancement of the local pinning (some individual atoms becoming more strongly pinned), and an increase in the interfacial commensurability (an increase in the number of atoms that are pinned in perfect synchrony). This is, to some extent, consistent with simulations of three-dimensional materials showing that interfacial commensurability, either through lattice matching<sup>20</sup> or through interaction-enhancing contaminant species, greatly increases static friction<sup>21</sup>. However, the evolution of interfacial friction and contact quality here is a result of high configurational freedom of graphene owing to its bending flexibility.

We then performed similar force analysis for multilayer ( $N=2-4$ ) graphene systems (see Supplementary Discussion 10) and found that the variation of the interfacial pinning and overall commensurability also contributed greatly to the layer dependence of friction, explaining the large quantitative disparity between the friction enhancement and true contact area increase in Fig. 1h. However, in the multilayer cases, the top graphene layer forms a perfect AB stacking with respect to the lower graphene layer. As observed in several experiments<sup>2,22</sup>, perfectly aligned stacking can strongly constrain the relative lateral movement of graphene layers. This enhanced constraint reduces the ability of graphene to adjust its configuration during the sliding process.

Since the contact interface with graphene can be affected by pre-existing wrinkles<sup>14</sup>, we speculate that regulating the degree of wrinkling<sup>23</sup> may offer an effective means of tuning friction. To test this, we studied a model system by sliding a tip over freely suspended graphene with various degrees of pre-existing wrinkling (Fig. 3a), formed by applying different amounts of bi-axial compressive strain ( $\epsilon_{xx}$  and  $\epsilon_{zz}$ ). Three samples G1, G2 and G3 with 0%,  $-0.2\%$ , and  $-0.5\%$  pre-compressive strain were studied in the simulations. As expected, the relaxation state of graphene profoundly affects its friction (Fig. 3b). Compared to G1, relaxed samples G2 and G3 exhibited substantially enhanced static friction (up to about 300%), although the increase in true contact area was much smaller (up to about 1.5%, see Fig. 3c). The  $f_i^{\text{friction}}$  distributions at the local force peaks of these three samples (Fig. 4a–c)

and their histograms (Fig. 4d) indicate that, as pre-compressive strain increased, stronger pinning sites with higher local interfacial forces appeared. Furthermore, the kurtosis analysis shows that the interfacial force distribution increasingly deviates from a unimodal Gaussian distribution from G1 to G3 (Fig. 4e), indicating a more commensurate interface with increasing pre-compressive strain.

As confirmed by the simulations, friction on suspended graphene can be effectively tuned by pre-compression and the ‘quality’ of the interfacial contact. But unlike the supported cases, the interface reached its steady configuration immediately after the tip made contact, because of larger excess area and resultant higher configurational flexibility. Thus, no frictional strengthening was observed in these simulations, consistent with the observations of Deng *et al.*<sup>11</sup>. We also performed simulations for graphene strongly bound to a flat surface. Owing to the much reduced freedom for graphene to configurationally evolve, no frictional strengthening or layer dependence occurred in this case either (see Supplementary Discussion 11), consistent with experimental measurements of strongly bound graphene<sup>8,24</sup>.

In conclusion, we have identified a complementary aspect to the concept of true contact area governing friction on two-dimensional materials, related to evolving configurational relaxations that exploit out-of-plane floppiness. There is a general tendency for configurationally flexible systems to attain progressively deeper energy traps despite mechanical work being done to the system, improving the quality of contact. Imposing pre-compression on suspended graphene (to produce wrinkles) increased the total friction force several times with little change in the true contact area. This suggests a means of controlling friction of two-dimensional materials via strain engineering.

**Online Content** Methods, along with any additional Extended Data display items and Source Data, are available in the online version of the paper; references unique to these sections appear only in the online paper.

**Received 16 February; accepted 30 September 2016.**

1. Szlufarska, I., Chandross, M. & Carpick, R. W. Recent advances in single-asperity nanotribology. *J. Phys. D* **41**, 123001 (2008).
2. Dienwiebel, M. *et al.* Superlubricity of graphite. *Phys. Rev. Lett.* **92**, 126101 (2004).

3. Filippov, A. E., Dienwiebel, M., Frenken, J. W. M., Klafter, J. & Urbakh, M. Torque and twist against superlubricity. *Phys. Rev. Lett.* **100**, 046102 (2008).
4. Kim, W. K. & Falk, M. L. Atomic-scale simulations on the sliding of incommensurate surfaces: the breakdown of superlubricity. *Phys. Rev. B* **80**, 235428 (2009).
5. van Wijk, M., Dienwiebel, M., Frenken, J. & Fasolino, A. Superlubric to stick-slip sliding of incommensurate graphene flakes on graphite. *Phys. Rev. B* **88**, 235423 (2013).
6. Li, Q., Tullis, T. E., Goldsby, D. & Carpick, R. W. Frictional ageing from interfacial bonding and the origins of rate and state friction. *Nature* **480**, 233–236 (2011).
7. Liu, Y. & Szlufarska, I. Chemical origins of frictional aging. *Phys. Rev. Lett.* **109**, 186102 (2012).
8. Lee, C. *et al.* Frictional characteristics of atomically thin sheets. *Science* **328**, 76–80 (2010).
9. Chhowalla, M. & Amaratunga, G. A. Thin films of fullerene-like MoS<sub>2</sub> nanoparticles with ultralow friction and wear. *Nature* **407**, 164–167 (2000).
10. Choi, J. S. *et al.* Friction anisotropy-driven domain imaging on exfoliated monolayer graphene. *Science* **333**, 607–610 (2011).
11. Deng, Z. *et al.* Nanoscale interfacial friction and adhesion on supported versus suspended monolayer and multilayer graphene. *Langmuir* **29**, 235–243 (2013).
12. Cho, D.-H. *et al.* Effect of surface morphology on friction of graphene on various substrates. *Nanoscale* **5**, 3063–3069 (2013).
13. Filleter, T. *et al.* Friction and dissipation in epitaxial graphene films. *Phys. Rev. Lett.* **102**, 086102 (2009).
14. Ye, Z., Tang, C., Dong, Y. & Martini, A. Role of wrinkle height in friction variation with number of graphene layers. *J. Appl. Phys.* **112**, 116102 (2012).
15. Smolyanitsky, A., Killgore, J. & Tewary, V. Effect of elastic deformation on frictional properties of few-layer graphene. *Phys. Rev. B* **85**, 035412 (2012).
16. Ishigami, M., Chen, J. H., Cullen, W. G., Fuhrer, M. S. & Williams, E. D. Atomic structure of graphene on SiO<sub>2</sub>. *Nano Lett.* **7**, 1643–1648 (2007).
17. Mate, C. M., McClelland, G. M., Erlandsson, R. & Chiang, S. Atomic-scale friction of a tungsten tip on a graphite surface. *Phys. Rev. Lett.* **59**, 1942–1945 (1987).
18. Bonelli, F., Manini, N., Cadelano, E. & Colombo, L. Atomistic simulations of the sliding friction of graphene flakes. *Eur. Phys. J. B* **70**, 449–459 (2009).
19. Li, Q., Lee, C., Carpick, R. W. & Hone, J. Substrate effect on thickness-dependent friction on graphene. *Phys. Stat. Sol. B* **247**, 2909–2914 (2010).
20. Luan, B. & Robbins, M. O. The breakdown of continuum models for mechanical contacts. *Nature* **435**, 929–932 (2005).
21. He, G., Müser, M. H. & Robbins, M. O. Adsorbed layers and the origin of static friction. *Science* **284**, 1650–1652 (1999).
22. Liu, Z. *et al.* Observation of microscale superlubricity in graphite. *Phys. Rev. Lett.* **108**, 205503 (2012).
23. Mohammadi, H. & Müser, M. H. Friction of wrinkles. *Phys. Rev. Lett.* **105**, 224301 (2010).
24. Spear, J. C., Custer, J. P. & Batteas, J. D. The influence of nanoscale roughness and substrate chemistry on the frictional properties of single and few layer graphene. *Nanoscale* **7**, 10021–10029 (2015).

**Supplementary Information** is available in the online version of the paper.

**Acknowledgements** S.L. and P.G. appreciate support from the Alexander von Humboldt Foundation and the Helmholtz Programme Science and Technology of Nanosystems (STN). Q.L., X.D. and J.S. appreciate support from the 973 Programs of China (grant numbers 2013CB933003, 2013CB934201, 2015CB351903 and 2012CB619402), the NSFC (grant numbers 11422218, 11272177, 11432008, 51320105014 and 51321003), the International Joint Laboratory for Micro/Nano Manufacturing and Measurement Technologies, the Tsinghua University Initiative Scientific Research Program (grant number 2014Z01007), the Thousand Young Talents Program of China and 111 project (grant number B06025). R.W.C. acknowledges support from the NSF (grant numbers CMMI-1401164 and MRSEC DMR-1120901). J.L. acknowledges support from the NSF (grant numbers MRSEC DMR-1120901, CBET-1240696, DMR-1410636 and ECCS-1610806). We also thank J. Feng for discussions.

**Author Contributions** Q.L., R.W.C. and J.L. conceived and designed the project. S.L. performed molecular dynamics simulations. Q.L., R.W.C. and X.Z.L. provided information about the atomic force microscope experiments. Q.L., P.G., X.D., J.S. and J.L. provided the simulation guideline. S.L., Q.L., R.W.C. and J.L. wrote the paper. All authors contributed to discussions and analyses of the results.

**Author Information** Reprints and permissions information is available at [www.nature.com/reprints](http://www.nature.com/reprints). The authors declare no competing financial interests. Readers are welcome to comment on the online version of the paper. Correspondence and requests for materials should be addressed to Q.L. ([qunyang@tsinghua.edu.cn](mailto:qunyang@tsinghua.edu.cn)), R.W.C. ([carpick@seas.upenn.edu](mailto:carpick@seas.upenn.edu)) or J.L. ([liju@mit.edu](mailto:liju@mit.edu)).

## METHODS

**Atomistic simulations.** In the molecular dynamics simulations, we primarily studied the stick–slip friction of a tip sliding on two graphene systems: multilayer graphene supported on a rough amorphous silicon (a-Si) substrate; and suspended monolayer graphene. The covalent bonds of C–C in graphene<sup>25</sup> and Si–Si in amorphous substrate and in the crystalline Si tip<sup>26</sup> were described using the Tersoff and Stillinger–Weber potentials, respectively. A typical 6–12 Lennard–Jones potential was employed to describe van der Waals adhesive interaction between graphene and the substrate, graphene and the tip, and between the graphene layers. The Lennard–Jones parameters were chosen such that the work of adhesion ( $E_{ad}$ ) or the pull-off force ( $f_{ad}$ ) obtained by the molecular dynamics calculation were at the same scale as those from experimental measurements<sup>11,16,27–29</sup>, as shown in Supplementary Table 1. The simulations were performed at 300 K using a Nosé–Hoover thermostat<sup>30</sup> with the LAMMPS<sup>31</sup> code. The atomic configurations are displayed using AtomEye<sup>32</sup>.

For the graphene/a-Si substrate system, we first created an a-Si substrate by quenching liquid silicon from high temperature to 300 K using a cooling rate of  $10^{13}$  K s<sup>-1</sup>. The lateral dimension of the substrate was  $43.4 \text{ nm} \times 43.4 \text{ nm}$  ( $x$ - $z$  plane) with a thickness of approximately 3.0 nm. The atoms in the lowest 0.5 nm were held fixed. Owing to the free boundary condition along the out-of-plane ( $y$ ) direction, roughness naturally formed on the free surface. A graphene sample,  $38.5 \text{ nm} \times 38.6 \text{ nm}$  in size was then placed above the a-Si within the adhesive interaction distance, and was then allowed to relax by approaching the substrate in response to adhesion. The root-mean-square roughness for the a-Si substrate and the relaxed graphene is 1.5 Å and 1.0 Å, respectively, close to experimental values<sup>33</sup>. After relaxation, a rigid (001)-oriented crystalline silicon tip in a bowl-shape with a radius of 16.3 nm is placed in contact with the graphene.

The rigid tip assumption was based on the following considerations. First, previous experiments<sup>8</sup> have demonstrated that the layer-dependent friction on graphene was reproducible regardless of the tip material (that is, silicon, silicon nitride, or diamond). Second, using a rigid tip that is non-deformable makes it easier to trace the important yet subtle evolution of the interfacial forces.

To incorporate the compliance of atomic force microscope cantilever in experiments, we coupled harmonic springs in the  $x$  direction for pulling the tip and in the  $z$  direction for applying a fixed normal force. The stiffness of the normal springs is  $30.0 \text{ N m}^{-1}$  and  $0.16 \text{ N m}^{-1}$ , comparable to the previous experiments<sup>8</sup>. The entire system was relaxed for 2 ns after adding the tip and further relaxed after the normal load was imposed. The friction tests were performed by displacing the lateral spring along  $x$  direction with a constant velocity of  $2 \text{ m s}^{-1}$  with a normal load of 0.8 nN applied, and calculating the lateral force acting on the virtual atom. To enhance the damping of oscillation (primarily along the lateral direction), we artificially decreased the tip mass by a factor of ten (see Supplementary Discussion 12). Simulations were performed at 300 K. Besides the rigid tip and the fixed atoms at the boundaries, all the other atoms in graphene and a-Si substrate were subjected to the thermostat. To further justify the rigid tip assumption, we carried out another simulation using a silicon tip sliding on monolayer graphene/a-Si substrate where all tip atoms were deformable but the topmost layer of atoms were rigid. We again obtained two-stage frictional behaviour (see Supplementary Discussion 13).

In the suspended graphene system, we created an ultraflat graphene sheet with dimensions of  $38.5 \text{ nm} \times 38.6 \text{ nm}$  in the  $x$ - $z$  plane. The boundaries were

non-periodic. To constrain translational movement during tip sliding, the atoms near the boundaries were fixed rigidly. The tip was the same as that used in the supported system. We coupled a harmonic spring with a lateral stiffness of  $30.0 \text{ N m}^{-1}$  and pulled the silicon tip at a velocity of  $2 \text{ m s}^{-1}$  in the  $x$  direction for friction tests. To minimize the boundary effects<sup>14</sup>, a small sliding distance of 2.5 nm was used, compared to the much larger width of the graphene sheet (about 39 nm). Again, the simulations were carried out at 300 K.

**Contact area.** The contact area between the tip and graphene is estimated by setting a cutoff distance  $r_c$  to judge whether graphene atoms are in intimate contact with the tip atoms. Here  $r_c = 4 \text{ Å}$ , which is slightly larger than the equilibrium distance of the Lennard–Jones potential imposed on the tip–graphene interaction. The contact area is then obtained by multiplying the total number of attached graphene atoms by the graphene atomic area of  $2.77 \text{ Å}^2$  per atom. It should be noted that the qualitative conclusions related to contact area are not affected even when we change the cutoff distance  $r_c$  slightly. For example, the 20% increase of  $r_c$  causes an increase of contact area by only 6%.

**Force analysis.** To minimize the influence of thermal fluctuation on interfacial forces, the force analyses were performed on quasistatic configurations which were obtained by further relaxing the system using the conjugate gradient method. This relaxation does not alter the frictional behaviour qualitatively, but it makes the statistical results more reliable and stable.

**Kurtosis.** The kurtosis is calculated as  $K = \mu_4/\sigma^4$ , where  $\mu_4$  is the fourth moment about the mean value and  $\sigma$  is the standard deviation of the distribution. Specifically,  $\mu_4 = \sum_n (f^{\text{friction}}(n) - \bar{f})^4 \rho(n)$  and  $\sigma^2 = \sum_n (f^{\text{friction}}(n) - \bar{f})^2 \rho(n)$ , where  $f^{\text{friction}}(n)$  is the atomic friction force of the  $n$ th bin,  $\rho(n)$  is the normalized atom number in each corresponding bin and  $\bar{f}$  is the mean value of  $f^{\text{friction}}(n)$  of all bins, where  $\bar{f} = \sum_n f^{\text{friction}}(n) \rho(n)$ . In our case, kurtosis measures the ‘peakedness’ and ‘tailedness’ of the force distribution.

**Data availability.** The authors declare that all data supporting the findings of this study are available within the paper and its Supplementary Information.

25. Tersoff, J. Empirical interatomic potential for carbon, with applications to amorphous carbon. *Phys. Rev. Lett.* **61**, 2879–2882 (1988).
26. Stillinger, F. H. & Weber, T. A. Computer simulation of local order in condensed phases of silicon. *Phys. Rev. B* **31**, 5262–5271 (1985).
27. Zacharia, R., Ulbricht, H. & Hertel, T. Interlayer cohesive energy of graphite from thermal desorption of polyaromatic hydrocarbons. *Phys. Rev. B* **69**, 155406 (2004).
28. Zong, Z., Chen, C.-L., Dokmeci, M. R. & Wan, K.-t. Direct measurement of graphene adhesion on silicon surface by intercalation of nanoparticles. *J. Appl. Phys.* **107**, 026104 (2010).
29. Koenig, S. P., Boddeti, N. G., Dunn, M. L. & Bunch, J. S. Ultrastrong adhesion of graphene membranes. *Nat. Nanotechnol.* **6**, 543–546 (2011).
30. Nosé, S. A unified formulation of the constant temperature molecular-dynamics methods. *J. Chem. Phys.* **81**, 511–519 (1984).
31. Plimpton, S. Fast parallel algorithms for short-range molecular dynamics. *J. Comput. Phys.* **117**, 1–19 (1995).
32. Li, J. AtomEye: an efficient atomistic configuration viewer. *Model. Simul. Mater. Sci. Eng.* **11**, 173 (2003).
33. Giannazzo, F., Sonde, S., Nigro, R. L., Rimini, E. & Raineri, V. Mapping the density of scattering centers limiting the electron mean free path in graphene. *Nano Lett.* **11**, 4612–4618 (2011).